Published in final edited form as:

Nat Med. 2017 February ; 23(2): 213–222. doi:10.1038/nm.4257.

Targeting the histone methyltransferase G9a activates imprinted genes and improves survival of a mouse model of Prader–Willi syndrome

Yuna Kim[1,9], **Hyeong-Min Lee**[2,3,9], **Yan Xiong**[4], **Noah Sciaky**[3], **Samuel W Hulbert**[5], **Xinyu Cao**[1], **Jeffrey I Everitt**[6], **Jian Jin**[4], **Bryan L Roth**[3,7], and **Yong-hui Jiang**[1,5,8]

[1]Department of Pediatrics, School of Medicine, Duke University, Durham, North Carolina, USA

[2]Department of Cell Biology and Physiology, University of North Carolina School of Medicine, Chapel Hill, North Carolina, USA

[3]Department of Pharmacology, University of North Carolina School of Medicine, Chapel Hill, North Carolina, USA

[4]Departments of Pharmacological Sciences and Oncological Sciences, Icahn School of Medicine at Mount Sinai, New York, New York, USA

[5]Department of Neurobiology, School of Medicine, Duke University, Durham, North Carolina, USA

[6]Department of Pathology, School of Medicine, Duke University, Durham, North Carolina, USA

[7]Program in Neuroscience, Division of Chemical Biology and Medicinal Chemistry, and NIMH Psychoactive Drug Screening Program, University of North Carolina School of Medicine, Chapel Hill, North Carolina, USA

[8]Program in Genetics and Genomics, School of Medicine, Duke University, Durham, North Carolina, USA

Abstract

Prader–Willi syndrome (PWS) is an imprinting disorder caused by a deficiency of paternally expressed gene(s) in the 15q11–q13 chromosomal region. The regulation of imprinted gene expression in this region is coordinated by an imprinting center (PWS-IC). In individuals with PWS, genes responsible for PWS on the maternal chromosome are present, but repressed epigenetically, which provides an opportunity for the use of epigenetic therapy to restore expression from the maternal copies of PWS-associated genes. Through a high-content screen

Correspondence should be addressed to B.L.R. (bryan_roth@med.unc.edu) or Y.-H.J. (yong-hui.jiang@duke.edu).

[9]These authors contributed equally to this work.

AUTHOR CONTRIBUTIONS

Y.K. and H.-M.L. designed and performed the experiments and wrote the manuscript. Y.X. and J.J. provided G9a inhibitors and epigenetic-small-molecule libraries. N.S. performed the Cell Profiler. B.L.R. supervised the high-content screening and provided small-molecule libraries. X.C. supported cell culture and mouse-colony maintenance. S.W.H. supported mouse-colony maintenance and neurological analysis. J.I.E. performed histopathological analysis. Y.J. designed the experiments and wrote the manuscript.

Note: Any Supplementary Information and Source Data files are available in the online version of the paper.

COMPETING FINANCIAL INTERESTS

The authors declare no competing financial interests.

(HCS) of >9,000 small molecules, we discovered that UNC0638 and UNC0642—two selective inhibitors of euchromatic histone lysine *N*-methyltransferase-2 (EHMT2, also known as G9a)—activated the maternal (m) copy of candidate genes underlying PWS, including the SnoRNA cluster *SNORD116*, in cells from humans with PWS and also from a mouse model of PWS carrying a paternal (p) deletion from small nuclear ribonucleoprotein N (*Snrpn* (*S*)) to ubiquitin protein ligase E3A (*Ube3a* (*U*)) (mouse model referred to hereafter as $m^{+}/p^{\Delta S-U}$). Both UNC0642 and UNC0638 caused a selective reduction of the dimethylation of histone H3 lysine 9 (H3K9me2) at PWS-IC, without changing DNA methylation, when analyzed by bisulfite genomic sequencing. This indicates that histone modification is essential for the imprinting of candidate genes underlying PWS. UNC0642 displayed therapeutic effects in the PWS mouse model by improving the survival and the growth of $m^{+}/p^{\Delta S-U}$ newborn pups. This study provides the first proof of principle for an epigenetics-based therapy for PWS.

PWS is clinically characterized by neonatal hypotonia and failure to thrive, childhood-onset obesity, intellectual disability and increased risk for psychosis in adults[1]. Although paternal deficiency of the 15q11–q13 chromosomal region is well documented as the etiology of PWS, the precise molecular basis underlying these clinical features remains elusive. Paternally expressed genes within 15q11–q13, including *SNRPN*, *MAGEL2*, *NDN* and *MKRN3*, and noncoding SnoRNA clusters of *SNORD115 (HBII-52*) and *SNORD116* (*HBII-85*), are controlled by a regulatory element defined as an imprinting center (PWS-IC)[2]. Among these genes, the SnoRNA cluster *SNORD116*, located between *SNRPN* and *UBE3A*, plays a critical part in PWS etiology, as indicated by genomic copy-number variant (CNV) analyses[3–6], and the specific role of *MAGEL2* in PWS remains a subject of debate owing to conflicting findings in humans[3,7–9].

SNORD116 is processed from its host transcript, a long noncoding RNA that is thought to initiate at the PWS-IC[10]. Human *SNORD116* and mouse *Snord116*, including host transcripts, are highly conserved in their genomic organization and imprinted expression patterns[10–12]; yet the mechanism underlying the imprinted expressions of *SNPRN* and *SNORD116* is still unclear. DNA methylation and histone modification are common mechanisms thought to be implicated in genomic imprinting. The differential methylation of CpG islands in the PWS-IC is consistent with the paternal activation of the genes, i.e., they are fully methylated on the maternal chromosome but unmethylated on the paternal chromosome[13]. However, histone modifications such as the acetylation of histone H3 lysine 4 (H3K4) and the methylation of histone H3 lysine 9 (H3K9) also exhibit allele-specific patterns in the PWS-IC[14,15]. Although histone modification is expected for transcriptional regulation, its role in the regulation of imprinted genes is less clear and has been viewed as an event secondary to, or as a substitute for, DNA methylation. DNA methylation inhibitors can activate the expression of the maternal-originated *SNRPN in vitro*[16], but this has not been reported *in vivo*. In addition, the inactivation of histone H3K9 methyltransferase G9a in mouse embryonic stem (ES) cells *in vitro* can induce the biallelic expression of *Snprn* that occurs with reduced DNA methylation[17]. Of note, DNA methylation of *Snrpn* is not affected in embryonic day 9.5 (E9.5) $G9a^{-/-}$ mouse embryos[17,18], yet the allele-specific expression of *Snrpn* in the absence of *G9a* is not known *in vivo*. Thus, we envisioned that epigenetic manipulation of the PWS imprinting domain could enable the maternal chromosome to

express PWS-associated genes that normally show paternal-specific expression, and thus provide a therapeutic strategy for PWS.

RESULTS

Identification of G9a inhibitors that activate candidate PWS-associated genes by a high-content screen

Our primary objective was to identify small molecules that are capable of activating the expression of *SNORD116* from the maternal chromosome, and so might offer therapeutic benefit for PWS. However, it was not feasible to design a screening for noncoding RNA. *SNRPN* (mouse *Snrpn*), however, is a protein-coding gene that is expressed paternally, but repressed maternally, in all tissues in human and mouse[19]. The allele-specific expression of human *SNRPN* is regulated by the PWS-IC, which also controls the expression of host transcripts for SnoRNAs, including the *SNORD116* cluster between *SNRPN* and *UBE3A*[20]. Thus, we decided to use the Snrpn-EGFP fusion protein (hereafter, S-EGFP) as a marker for a HCS campaign. We reasoned that small molecules that can activate S-EGFP might also be effective at activating the host transcript of *Snord116*. Accordingly, we established mouse embryonic fibroblasts (MEFs) from mice carrying S-EGFP inherited either maternally ($m^{S\text{-}EGFP}/p^{+}$) or paternally ($m^{+}/p^{S\text{-}EGFP}$), in which *EGFP* is inserted after exon 2 of the *Snurf–Snrpn* bicistronic transcript[21]. We confirmed that S-EGFP was expressed in $m^{+}/p^{S\text{-}EGFP}$ and repressed in $m^{S\text{-}EGFP}/p^{+}$ MEFs (Supplementary Fig. 1a). The MEFs of $m^{S\text{-}EGFP}/p^{+}$ were then subjected to a HCS using a protocol that we described previously[22] (Fig. 1a). We performed the screen in quadruplicate, using 13 small-molecule libraries from multiple sources, including three random epigenetic-library collections (10 μM in 0.2% DMSO; Fig. 1b and Supplementary Table 1). We chose these libraries to ensure chemical diversity and pharmacological and biological activity. After employing an initial arbitrary cut-off of 125% (100% indicates basal fluorescence in the vehicle-treated MEFs), out of 9,157 compounds (Fig. 1b), we identified 32 potentially active compounds from the primary screen (Supplementary Fig. 1b and Supplementary Table 2). Two of these compounds, UNC0638 and UNC0642, were validated and shown to be active in orthogonal assays of immunocytochemistry (Fig. 1c), concentration responses (Fig. 1d) and quantitative reverse transcription PCR (RT–qPCR) (Fig. 1e).

Both UN0638 and UNC0642 have been characterized as G9a- selective inhibitors that bind and block the catalytic domain of G9a[23,24]. Through an extended screening of 23 UNC0638 and UNC0642 analogs, we subsequently identified two additional compounds: UNC617 (Supplementary Fig. 2) and UNC618 (ref. 25) that could also activate the expression of S-EGFP in $m^{S\text{-}EGFP}/p^{+}$ MEFs (Fig. 1c–e). UNC0638, UNC0642 and UNC617 displayed similar potencies in concentration-response studies (Fig. 1d; half-maximal effective concentration (EC_{50}) = 1.6 μM for UNC0638, 2.7 μM for UNC0642 and 2.1 μM for UNC617). The estimated maximal effectiveness (E_{max}) was similar for these three compounds, whereas UNC618 was effective only at 30 μM. Next, we performed RT–qPCR to measure the changes in mRNA of S-EGFP. These compounds upregulated the mRNA of S-EGFP to an extent comparable to or greater than that induced by 10 μM of 5-aza deoxycytidine (5-Aza-dC), an inhibitor of DNA methyltransferases (DNMTs) (Fig. 1e).

Because other allele-specific histone modifications, such as acetylation, occur in the PWS-IC[16], we next examined whether the modulation of other classes of histone-modifying enzymes can activate S-EGFP. However, as summarized in Supplementary Table 3, we did not observe activation of S-EGFP in the presence of different classes of modulators. Notably, BIX01294 (ref. 26), the first reported G9a inhibitor, which is less potent than UNC0638 and UNC0642, did not have a substantial effect on the activation of S-EGFP (Supplementary Table 3). These data suggest that the effects of our active compounds are relatively specific and probably result from targeting specific histone methyltransferases.

Next, we tested whether these drugs could derepress the maternal genes in a patient-driven cell model of PWS: a human skin fibroblast cell line containing a typical large 5–6-Mb deletion of the paternal copy of the 15q11–q13 region (Fig. 2a). Because imprinting of *SNRPN* is known to be ubiquitous[19], the G9a-inhibitor effect on its activation is expected to be representative of all tissues and cell types. Using the indicated treatment scheme (Fig. 2b), we compared the effectiveness of four identified compounds from the HCS, including a control, 5-Aza-dC. All of them displayed apparent activation of *SNRPN* mRNA expression from the maternal chromosome (Fig. 2c). However, only UNC0638 and UNC0642 were effective for *SNORD116* and the putative host transcripts for *SNORD116* (*116HG*) and *SNORD115* (*115HG*). For *116HG*, multiple bands were seen in the drug-treated cells, and these products were further examined through subsequent Sanger sequencing. As indicated, some of these products were mapped to the region of *116HG* (Fig. 2c), and the majority of the sequences were not specific or partially matched to the long-terminal-repeat sequence, a known sequence that requires G9a for its repression[27]. The UNC0638 and UNC0642 treatments also reactivated the expression of *NDN*, which is 1 Mb proximal to PWS-IC. We were not able to determine the expressions of *MAGEL2* and *SNORD115*, despite the activation of *115HG*, because they are not normally expressed in skin fibroblasts[28–30].

We chose UNC0638 for follow-up cell-based studies because of its high potency and selectivity, low toxicity and thoroughly characterized cellular activity[23]. UNC0638 treatment (1–4 μM) effectively activated *SNRPN* and *SNORD116* transcripts, as assessed by RT–PCR (Fig. 2d), with minimal cytotoxicity (Supplementary Fig. 3). PWS fibroblasts treated with 4 μM of UNC0638 expressed approximately 30% of control SNRPN protein levels (Fig. 2e and Supplementary Fig. 4). Taken together, these expression analyses strongly indicate that UNC0638 and UNC0642 are capable of activating the maternal copy of the paternally expressed genes from the PWS-associated region.

G9a inhibitors improved survival and growth in a mouse model of PWS

Using the $m^{+}/p^{\Delta S-U}$ mouse model of PWS[31], we next examined the effects of UNC0642 *in vivo*. Neonatal $m^{+}/p^{\Delta S-U}$ mice display perinatal lethality and poor growth[31] that resembles the failure-to-thrive feature of individuals with PWS during the first year of life[1]. We chose UNC0642 because it has not only high potency and selectivity for G9a in biochemical and cellular assays, but also excellent pharmacokinetic (PK) properties, including CNS penetration superior to UNC0638 (ref. 24). A single intraperitoneal (i.p.) injection dose of 5 mg/kg of UNC0642 is sufficient to inhibit G9a activity in adult mice[24]. We administered the G9a inhibitor UNC0642 in a blinded and randomized fashion to mouse genotypes between

postnatal day 7 (P7) and P12, because most $m^{+}/p^{\Delta S-U}$ pups died before weaning. For neonatal mice, we used a lower dosage regimen of 2.5-mg/kg i.p. injections for 5 consecutive days (Fig. 3a). The UNC0642 treatment was well tolerated by both wild-type (WT) and $m^{+}/p^{\Delta S-U}$ pups and significantly attenuated lethality in $m^{+}/p^{\Delta S-U}$ mice as compared to the untreated $m^{+}/p^{\Delta S-U}$ group (Fig. 3b). The difference in the survival rates of PWS pups was most notable during the first week after drug administration and diminished over time. Six UNC0642-treated $m^{+}/p^{\Delta S-U}$ pups survived to >P90 (15%; $n = 40$), and they had normal physical appearance (Fig. 3c) and activity in their home cages. Body-weight measurements revealed that there was a significant improvement of growth between P10 and P19 in treated $m^{+}/p^{\Delta S\text{-}U}$ pups (Fig. 3d). These results indicate the—albeit partial—rescue of lethality and growth-delay phenotypes of the PWS mouse model, and hence the potential of such treatment for humans.

To assess the potential toxicity associated with UNC0642 treatment, we monitored body weight in WT groups. Notably, loss of body weight, a sign of general health deficiency, was not observed in WT mice treated with UNC0642 (Fig. 3e). We also performed a general health and neurological screening in a blinded fashion, and it did not reveal any substantial abnormalities (Supplementary Table 4). In additional toxicity tests, we did not include vehicle-treated PWS mice because of the small sample size. Despite our breeding effort that produced a total number of 60 $m^{+}/p^{\Delta S-U}$ pups, only two vehicle-treated $m^{+}/p^{\Delta S-U}$ mice survived to P90. In hematological analysis, the measurements of treated $m^{+}/p^{\Delta S-U}$ and WT mice were within normal ranges, as measured by liver and kidney functions as well as normal lipid and protein metabolism, which are indicative of normal health conditions (Supplementary Table 5). Histopathological analyses also did not reveal any abnormalities associated with UNC0642 treatment in the brain, liver, kidney, lung and heart from mice at P90, both in $m^{+}/p^{\Delta S-U}$ and WT mice (Supplementary Fig. 5).

We next assessed RNA and protein expression in $m^{+}/p^{\Delta S-U}$ mice at around P14 following UNC0642 treatment (Fig. 4a). The expression of *Snrpn* and *Snord116* was readily detectable in the brain and liver—two organs relevant to the pathogenesis of PWS—of UNC0642 treated $m^{+}/p^{\Delta S-U}$ mice by RT–PCR (Fig. 4b) and quantitative reverse transcription PCR (RT–qPCR) (Fig. 4c), whereas vehicle-treated $m^{+}/p^{\Delta S-U}$ mice had no detectable transcripts (Fig. 4b,c). We also examined whether this activation affects the maternal expression of *Ube3a* because its antisense transcript (*Ube3a*-ATS), which has an essential role in repressing the paternal copy of *Ube3a* in the brain, is also only paternally expressed[32,33]. Notably, the expression of *Ube3a*-ATS was not affected in the brain (Fig. 4c). Similarly, the Ube3a protein level was not changed in whole brain (Fig. 4d), or specifically, in the cerebellum, where the maternal-specific *Ube3a* transcript is predominantly expressed[34] (Supplementary Fig. 6). We also accessed the treatment effect in adulthood using the $m^{S\text{-}EGFP}/p^{+}$ mouse model (Fig. 4e–g). Treatment of 6-week-old mice exerted a long-lasting effect, as shown by the maternal expression of *Snrpn–EGFP* at 0 (Fig. 4f), 1, 4 and 12 weeks (Fig. 4g) after the final dose of UNC0642. However, it is worth noting that expression levels at 12 weeks were significantly lower than those at 4 weeks ($P = 0.03$). Therefore, these results demonstrate the efficacy of UNC0642 treatment *in vivo* for the mouse model of PWS and provide sufficient proof of principle to consider evaluating such a therapeutic intervention, targeted at the molecular etiology of PWS.

G9a inhibitors affected H3K9 methylation but not DNA methylation in PWS domain

We next investigated the underlying mechanism for the activation of the maternal chromosome 15q11–q13 by UNC0638 and UNC0642. The PWS-IC is methylated on the maternal chromosome, but unmethylated on the paternal chromosome[2]. This allele-specific methylation is thought to implicate the imprinted regulation of candidate PWS-associated genes[14,16]. Given that G9a is also known to modulate DNA methylation via the ankyrin-repeat domain (ANK) but not the catalytic domain of G9A[35,36], we first examined the differential methylation to see whether the activation of the maternal genes by the G9a inhibitors occurs directly or through the loss of DNA modification. As expected, 5-Aza-dC significantly decreased DNA methylation of the PWS-IC as compared to the vehicle-treated group when examined by a bisulfite genomic-sequencing method ($P < 0.05$). By contrast, the UNC0638 and UNC0642 did not significantly alter DNA methylation of the PWS-IC in human PWS cells or in $m^{+}/p^{\Delta S-U}$ mice, respectively, as analyzed by the bisulfite genomic-sequencing method (Fig. 5a), which is in agreement with the previous report showing that UNC0638 does not alter global DNA methylation[23]. These data suggest that maternal activation is partially independent from the loss of DNA methylation, even though a dose-dependent hypomethylation of long terminal repeats (LTRs) for individual genomic loci was observed in UNC0638-treated cells[23].

We next examined whether these inhibitors affected the H3K9 methylation pattern. Both H3K9me2 (dimethylation of H3K9)[15,17] and H3K9me3 (trimethylation of H3K9)[37] are associated with the maternal chromosome in the PWS region. We verified differential histone modifications of the PWS-IC by a chromatin immunoprecipitation (ChIP) assay, in which H3K9me2 and H3ac (acetylation of H3) were enriched at the maternal or paternal PWS-IC, respectively (Supplementary Fig. 7). We also noted that treatment with 5-Aza-dC also reduced H3K9me2 in the PWS-IC of the maternal chromosome as compared to the vehicle-treated group (Supplementary Fig. 7). The suppression of DNA methylation thus seems to impair H3K9 methylation at the PWS-IC, possibly owing to the loss of interaction between DNMTs and G9a[35,36]. Using the *MAGE-A2* promoter[38] and a centromere sequence (CEN)[15] as controls, UNC0638 drastically reduced the levels of H3K9me2 and H3K9me3 in the PWS-IC and *SNORD116* regions (Fig. 5b,c). H3K9me2, but not H3K9me3, was enriched at the PWS-IC, and treatment with UNC0638 reduced H3K9me2 as compared to the untreated control cells in PWS-IC (Fig. 5b,c). The UNC0638 treatment also reduced H3K9me2 of other examined sites along the PWS region, including the promoter of *NDN* (Supplementary Fig. 8). At the region of the host transcript of *SNORD116*, both H3K9me2 and H3K9me3 were enriched, and UNC0638 treatment reduced H3K9me2 (Fig. 5b,c) and H3K9me3 (Fig. 5b,d) as compared to the untreated controls.

Although G9a catalyzes primarily mono- and dimethylation reactions on H3K9 by its Su(var)3-9 and enhancer of zeste (SET) domain, it can contribute to the trimethylation of H3K9 in individual loci via an undefined biochemical mechanism[39,40]. This undefined regulation might account for the changes in H3K9me3 at the *SNORD116* region. Despite the reduction of H3K9me2 at the *MAGE-A2* promoter, we did not see the transcriptional activation *of MAGE-A2* (Supplementary Fig. 9a). This is probably because *MAGE-A*2 activation by G9a inhibitors is cell type– and treatment condition–dependent[23,26]. We also

tested the effects of the G9a inhibitor on the other imprinted loci, including maternally expressed *CDKN1C*, and paternally expressed *IGF2* and *PEG10*. We found that the expression of only the paternally expressed *PEG10* was modestly upregulated by the G9a inhibitor (Supplementary Fig. 9b). This suggests that the inhibition of G9a affects gene expression in a locus-selective manner, and this is consistent with the study reporting that only 1 of 16 imprinted loci are selectively affected in *G9a*$^{-/-}$ embryos[18].

We next performed G9a chromatin immunoprecipitation (ChIP) analysis. G9a recognizes H3K9me2 through its ANK domains, which might amplify the spreading of H3K9me2 (refs. [41,42]). The associations of G9a with the PWS-IC and *SNORD116* region were not significantly affected (Fig. 5e), which indicates that UNC0638 does not impair the binding of G9a to chromatin. Given that DNA methylation did not change in the presence of the G9a inhibitors, it might further suggest that the intact protein–protein interaction between ANK and DNMTs can still be capable of modulating DNA methylation. This idea is supported by previous reports showing that the ANK domain, but not the catalytic domain, of G9a is essential to maintaining the DNA methylation of imprinted genes[35,43].

G9a-inhibitor treatment led to more open chromatin in the PWS imprinted domain

H3K9me2 facilitates heterochromatin formation to regulate transcription[38,40]. We thus investigated whether the reduction of H3K9 methylation could result in more open chromatin across the imprinted domain. Quantitative PCR of genomic DNA following *in situ* nuclease digestion was performed to measure chromatin accessibility (Fig. 6a), using a previously described protocol[44]. We used the following controls in this study: the constitutively expressed *GAPDH*, which was highly susceptible to nuclease digestion, and constitutively silent rhodopsin, which displayed minimal chromatin accessibility, regardless of UNC0638 treatment (Supplementary Fig. 10). As a result of the treatment with UNC0638, the target regions across the imprinted domains, including the *SNRPN* and *SNORD116*, were more open and accessible than vehicle-treated controls (Fig. 6b). The effect of UNC0638 and UNC0642 seemed to be bidirectional in reference to the PWS-IC in the PWS domain.

Taken together, these results suggest that the reduction of H3K9 methylation, but not DNA demethylation of PWS-IC, by the UNC0638 and UNC0642 treatment leads to more open chromatin, which, in turn, activates candidate PWS-associated genes from the maternal chromosome (Fig. 6c).

DISCUSSION

We discovered that the G9a inhibitors UNC0638 and UNC0642, identified from an unbiased small-molecule HCS, activate the candidate PWS-associated genes from the maternal chromosome both in human PWS patient-derived cells and in a mouse model of PWS. Treatment with UNC0642 afforded a clear therapeutic benefit for PWS-related phenotypes, including perinatal lethality and poor growth, which resemble the common clinical features of failure to thrive in individuals with PWS during the first year of life[31]. Further studies are necessary to determine whether G9a inhibitors might offer therapeutic benefit to other major

clinical problems of PWS, such as obesity, hyperphagia and behavioral impairment, that occur in childhood or later[1], when appropriate animal models of PWS become available.

We also show that UNC0642 treatment does not affect the expression of *Ube3a*, a maternally expressed gene whose loss causes Angelman syndrome (AS). The activation of PWS-associated genes on the maternal chromosome raises a concern because it may activate *Ube3a* antisense RNA (*Ube3a*-ATS), which normally represses paternal *Ube3a* expression[32,33] but is not expressed from the maternal chromosome[45]. It is unclear how the derepression of the PWS-associated genes *Snrpn* and *Snord116* occurs without affecting the expression of *Ube3a*-ATS. The generation and the processing of host transcripts from the interval between PWS-IC and *Ube3a* are not well understood. In contrast to the current notion of a long transcript *IC-SNURF-SNRPN*[10], we speculate that the expressions of *Snord116* host transcript and *Ube3a*-ATS are regulated differently. A recent study in human tissues from healthy individuals found potential transcription start sites (TSSs) within the interval between PWS-IC and *UBE3A* (ref. 46): one between *SNORD116* and *SNORD115* clusters and another between *SNORD115* and the 3′ end of *UBE3A*. The large host transcript from the PWS-IC, which overlaps with the *SNRPN* promoter, might stop before these additional TSSs, and *UBE3A*-ATS might be initiated from one of potential TSSs, probably the one close to the 3′ end of *UBE3A*. It seems that our G9a-inhibitor treatment derepresses the PWS-IC overlapping with *Snrpn* promoter, but not the TSS of *Ube3a*-ATS on the maternal chromosome. The continuous distribution of H3K9me2 along the PWS domain does not extend to the distal region[47], which then makes the TSS of *Ube3a*-ATS not targetable by the G9a inhibitor. Another possibility is that the effect of the G9a inhibitor might become weaker at the farther end distal to the PWS-IC.

It is not well understood how the functions of histone methylation and DNA methylation are linked for the repression of the PWS-associated imprinting domain *in vivo*. A previous genetic study showed that the PWS-IC was demethylated in *G9a*-deficient embryonic stem (ES) cells, whereas it was not affected in G9a-deficient mouse embryos[17]. Unfortunately, the expressions of PWS-associated genes have not been examined specifically in G9a-deficient embryos (which died at E9.5)[38], presumably owing to technical difficulties associated with determining their allele-specific expression in embryonic tissue. We demonstrate that the repressed *SNRPN* and *SNORD116* are activated by the pharmacological inhibition of G9a, and that the reactivation occurred without any alteration of DNA methylation (5-methylcytosine, 5mC) of the PWS-IC both *in vitro* and *in vivo*. It should be noted that the possibility of modifications other than 5mC in PWS-IC being affected by the G9a inhibitor cannot be ruled out because the bisulfite method used for our DNA-methylation analysis cannot distinguish between 5mC and 5-hydroxymethylcytosine (5hmC), or between cytocine (C) and 5-carboxycytosine (5CaC)[48–50]. Nevertheless, the finding provides novel insights into the regulation of imprinting, whereby H3K9 methylation has a decisive role in the repression of PWS-associated genes on the maternal chromosome.

We propose a chromatin-spreading model for the maternal activation of PWS-associated genes, in which a reduction of H3K9 methylation is sufficient for altering the chromatin state so that it becomes permissive to transcriptional activation. Previous genome-wide chromatin profiling has revealed the regions of large, organized chromatin K9 modification

(LOCK), including one from *MKRN3* to the 3′ end of *UBE3A* in the PWS-associated imprinted domain[47]. We underscore in the model that reduced H3K9me2 in the PWS-IC initiates the spread of open chromatin along the PWS-associated imprinted region. However, our data do not rule out another possibility, wherein the reduced H3K9 methylation in the individual loci across the imprinted domain could also contribute to more open chromatin after G9a-inhibitor treatment.

Our findings provide a proof of principle to develop small-molecule-based epigenetic therapy for human PWS (Fig. 6d). From a translational perspective, the G9a inhibitor UNC0642 improves the life span and weight gain of $m^{+}/p^{\Delta S-U}$ pups, produces long-lasting activation of PWS-associated genes, is apparently well tolerated and produces no notable acute toxicity, and does not interfere with the expression of the AS-associated *Ube3a* gene. For the development of new drug therapy, potential off-target effects associated with epigenetic drugs raise a general safety concern. The well-tolerated response to UNC0642, however, suggests that each case may be evaluated individually with careful consideration to the dose, duration, route and timing of drug delivery. The tolerability of the US Federal and Drug Administration–approved DNA-methylation inhibitor, observed in patients with myelodysplastic syndrome, is one example of the safety of an epigenetic drug[51,52]. It is also noteworthy that, in reported human cases, the disruption of multiple imprinted loci as a result of mutations in zinc-finger protein 57 (*ZFP57*), a transcriptional factor, result in only a relatively rare but mild condition of transient neonatal diabetes[53,54], and suggests a more complex possibility for evaluating the broad effects of epigenetic drugs. Our study provides a crucial step toward the development of a specific molecular therapy for human PWS. On the basis of these promising results, comprehensive evaluation of the efficacy and tolerability of G9a inhibitors in preclinical studies is warranted to fully explore their therapeutic potential for treating PWS.

METHODS

Methods, including statements of data availability and any associated accession codes and references, are available in the online version of the paper.

ONLINE METHODS

Animals

We handled all animals for all experiments with an Institutional Animal Care and Use Committee (IACUC) protocol approved by Duke University. *Snrpn-EGFP* mice[21] and the PWS mouse model with a paternal deletion from *Snrpn* to *Ube3a* ($m^{+}/p^{\Delta S-U}$)[31] were previously described. We maintained *Snrpn-EGFP* mice on C57BL/6J and mice with a deletion from *Snrpn to Ube3a* (*ΔS–U*) on C57B6/J and 129/SvEv mixed background. We produced $m^{+}/p^{\Delta S-U}$ mice and its littermates by crossing wild-type females to heterozygous $m^{\Delta S-U}/p^{+}$ male mice. Male and female mice were used in all studies.

Cell culture

To generate primary mouse embryonic fibroblasts (MEFs) carrying maternal Snrpn-EGFP ($m^{S\text{-}EGFP}/p^{+}$), we crossed *Snrpn-EGFP*/+ heterozygous females with wild-type males and

we isolated embryos at E12.5 to E14.5. In addition, we isolated MEFs carrying paternal Snrpn-EGFP ($m^{+}/p^{S\text{-}EGFP}$) from the embryos of wild-type females crossing with *Snrpn-EGFP*/+ heterozygous males. We obtained human fibroblasts from patients with PWS from the Baylor College of Medicine cell repository and NIGMS Human Genetic Mutant Cell Repository. We maintained MEFs in Dulbecco's modified Eagle's medium (Gibco 11995-065) supplemented with 10% FBS (Gibco 10082-147), 1% gentamicin (Gibco 15710-064), 1% glutamine (Gibco 25030-149), 1% nonessential amino acid (Gibco 11140-050), 0.1% β-mercaptoethanol (Gibco 21985-023), 100 units/ml penicillin and 100 μg/ml streptomycin (Gibco 15240-062) at 37 °C and 5% CO_2. We maintained human fibroblast cells in minimum essential medium alpha media (Gibco 12571-063) supplemented with 10% FBS (Gibco 10082-147), 1% L-glutamine (Gibco 25030-081), 100 units/ml penicillin and 100 μg/ml streptomycin (Gibco 15240-062) at 37 °C and 5% CO_2.

High-content screening of small-molecule libraries

We performed high-content screening of small molecules according to the previous study[22]. Briefly, we isolated primary MEFs from E12.5–14.5 embryos of Snrpn-EGFP mice as described above. We maintained fibroblasts in Dulbecco's modified Eagle's medium supplemented with 10% FBS, 100 units/ml penicillin and 100 μg/ml streptomycin, at 37 °C and 5% CO_2. 1 d before treatment with small molecules, we plated 5,000 cells per well onto 384-well plates. On the next day, we performed screening in quadruplicate using multiple small-molecule libraries (Supplementary Table 1) and a compound concentration of 10 μM in 0.2% DMSO vehicle. 3 d after drug treatment, we imaged the immunofluorescence-processed fibroblasts for Hoechst and AlexaFluor 488 fluorescence using a BD Pathway 855 high-content imaging microscope. We determined antibody-enhanced S-EGPF fluorescence intensity in drug-treated cells individually and normalized to cells treated with vehicle control. We performed analysis using Cell Profiler[55] with custom macro and algorithms. We defined potential active drugs as the increase in drug-mediated EGFP fluorescence observed consistently across quadruplicate wells and minimal or no cytotoxicity measured by Hoechst-stained nuclear structure (and the changes in total number of cells). After initial validation of all potential active drugs (for example, to determine whether active compounds show inherent fluorescence, the wild-type fibroblasts were also treated), we further validated only effective hit compounds in dose-response tests to determine relative efficacy (E_{max}) and potency (EC_{50}). We analyzed the dose-response results by using Graphpad Prism (Graphpad Software). The calculated EC_{50} values (potencies) and estimated E_{max} (efficacy, y value top plateau) enabled comparative analyses of the relative potency and efficacy of the identified compounds.

In vitro and *in vivo* drug treatment

We cultured human fibroblast cells to ~80% confluence and treated them with compounds (UNC617, UNC0638 and UNC0642 at 4 μM; UNC618 at 8 μM; or 5-aza-dC at 10 μM final concentration) diluted in culture medium for 72 h. For treatment in the PWS model, we performed daily intraperitoneal (i.p.) injections to $m^{+}/p^{\Delta S-U}$ litters starting at P7 and then for the following 5 d (UNC0642 (2.5 mg/kg), diluted in isotonic saline solution (PBS) containing 0.02% DMSO). We genotyped pups at the time of weaning or after their death. Mice of both sexes were used, and the mouse sex information is listed in Supplementary

Table 4. For testing chronic drug effects, we performed daily i.p. injection to 6-week-old $m^{S\text{-}EGFP}/p^{+}$ female mice for 7 consecutive days.

General chemistry procedure

Syntheses of UNC618, UNC0638 and UNC0642 were reported previously[23–25]. We acquired HPLC spectra for UNC617 using an Agilent 6110 Series system with UV detector set to 254 nm. We injected samples (5 μl) onto an Agilent Eclipse Plus 4.6 × 50 mm, 1.8 μM, C18 column at room temperature. A linear gradient from 10% to 100% B (MeOH + 0.1% acetic acid) in 5.0 min was followed by pumping 100% B for another 2 min with A being H_2O + 0.1% acetic acid. The flow rate was 1.0 m/min. We acquired mass spectra (MS) data in positive-ion mode using an Agilent 6110 single-quadrupole mass spectrometer with an electrospray ionization (ESI) source. We acquired high-resolution mass spectra (HRMS) using an Aglient 6210 LCMS orthogonal-axis time-of-flight (TOF) mass spectrometer. We recored nuclear magnetic resonance (NMR) spectra at Varian Mercury spectrometer with 400 MHz for proton (1H NMR) and 100 MHz for carbon (^{13}C NMR); chemical shifts are reported in p.p.m. (δ). We performed preparative HPLC on Agilent Prep 1200 series with UV detector set to 220 nm. We injected samples onto a Phenomenex Luna 75 × 30 mm, 5 μM, C18 column at room temperature. The flow rate was 30 ml/min. We used a linear gradient with 10% of MeOH (A) in 0.1% TFA in H_2O (B) to 100% of MeOH (A). We used HPLC to establish the purity of target compounds.

Immunoblotting

We performed western blot analyses as previously described[56]. Briefly, we extracted total protein from collected tissues (liver and brain from P14–P15 mice) using modified RIPA buffer (1 × PBS, 1% Triton X-100, 0.1% SDS, 2 mM EDTA, and protease inhibitors). SDS–PAGE resolved 25 μg of total proteins, and we transferred it to polyvinylidene difluoride (PVDF) membranes. We blocked the PVDF membranes with BLOTTO (5% skim milk and 0.1% Tween-20 in 1× TBS buffer), and incubated with primary target antibodies, rabbit anti-Snrpn (Protein Tech, cat. no. 11070-1-AP) at 1:400, and rabbit anti-Ube3a (Bethyl Lab, cat. no. A300-352A-T) at 1:1,000 working concentration in BLOTTO at 4 °C overnight. The next day, following incubation with horseradish peroxidase-conjugated secondary antibodies, we incubated the membranes with a Pierce chemiluminescent substrate and exposed it to X-ray film or imaged it by AI600 (GE Healthcare Life Science).

Immunocytochemistry

We performed immunofluorescence staining to detect any upregulated Snrpn-EGFP. 3 d after drug treatment, we fixed the cells with 4% paraformaldehyde at room temperature for 10 min, followed by rinsing with 1× PBS. We permeabilized the cells with 0.5% Triton X-100 in 1× PBS at room temperature for 10 min, followed by blocking with 5% normal goat serum in 0.1% Triton X-100 in 1× PBS at room temperature for 30 min. We incubated primary rabbit anti-GFP antibody (1:1,000, Novus Biologicals cat. no. NB100-1770) at 4 °C overnight. The next day, we rinsed the cells with 1× PBS and incubated with goat anti-rabbit AlexaFluor 488 (Invitrogen cat. no. A-11008) and Hoechst at room temperature. 1 h after incubation, we rinsed the cells with 1× PBS and imaged for Hoechst and AlexaFluor 488 fluorescence using a BD Pathway 855 high-content imaging microscope.

Cell-viability assay

We analyzed cell viability measured by fluorescence using CellTox Green Cytotoxicity Assay (Promega, cat. no. G8741), according to the manufacturer's instructions.

Histopathological analysis

We fixed brain, liver, lung, kidney and heart tissues from 3-month-old mice in 10% neutral buffered formalin (NBF: 10 ml of Formalin (37% stock), 90 ml of deionized water, 4 g/liter of NaH_2PO_4, 6.5 g/liter Na_2HPO_4), embedded them in paraffin, sectioned them at 5 μm, stained them with hematoxylin and eosin and then had a board-certified toxicological pathologist examine the images.

Blood chemistry and hematological analysis

We collected blood from 3-month-old mice into microcontainers or hematology assay tubes using jugular vein bleeding puncture. We obtained a serum metabolic panel using the Heska Dry Chem analyzer (Cuattro Veterinary USA). The metabolic panel contained chem and electrolyte, liver and kidney functions. For hematology analysis, we tested whole blood using Procyte (IDEXX).

Gross neurological screening

We evaluated general health using a modified version of standard test battery for behavioral phenotyping of mice[57]. Observational assessment included the evaluation of body weight, body core temperature, overt behavioral signs (coat appearance, body posture and secretary signs) and sensory functions (visual ability, audition, tactile perception and vestibular function). Supplementary Table 4 indicates the mouse sex and age information.

RT–PCR and RT–qPCR

For reverse-transcription PCR (RT–PCR) and quantitative real-time RT–PCR (RT–qPCR), first we extracted total RNA from the fibroblasts and/or collected tissues (liver and brain from P14–P15 mice and 7, 10 and 18-week-old $m^{+}/p^{S\text{-}Egfp}$ mice) using Direct-zol RNA Miniprep kit (Zymo Research cat. no. R2070). We directly used 2 μg of total RNA for single-strand cDNA synthesis with Superscript III reverse transcriptase (Invitrogen cat. no. 18080-093) according to the manufacturer's protocols. The conditions for RT– PCR was 95 °C/5 min, 35–40 cycles of 95 °C/30 s, 56–60 °C/60 s, 72 °C/60 s. We performed quantification of target gene expression in a LightCycler480 instrument (Roche) using SsoAdvanced Universal SYBR green Supermix (Biorad cat. no. 172-5271) according to the manufacturer's instructions. The primers that we used in this study are listed here. *SNRPN* (forward, 5′-gctgcagcacattgactatagaat-3′; reverse, 5′-cacagtcatggataccaagttctc-3′), *SNORD116* (forward, 5′-tggatcgatgatgagtcc-3′; reverse, 5′-tggacctcagttccgatgaga-3′), *116HG* (forward, 5′-ctggtggatcccacaggt-3′; reverse, 5′-agaagcccacgccacata-3′), *115HG* (forward, 5′-cttcctcacaccctggtctc-3′; reverse, 5′-gacttcaagaaatgcgtgctc-3′), *NDN* (forward, 5′-ggggtgggtcattatagtattcag-3′; reverse, 5′-acaaaaatccaagaaaggtagcac-3′), *MAGEL2* (forward, 5′-ctaagaagctcatcaccgaag-3′; reverse, 5′-ggcagatacgaaaccaagttg-3′), β-actin (forward, 5′-agagctacgagctgcctgac-3′; reverse, 5′-agcactgtgttggcgtacag-3′), *mSnrpn* (forward, 5′-ttggttctgaggagtgatttgc-3′; reverse, 5′-ccttgaattccaccaccttg-3′), *mSnord116*

(forward, 5′-ggatctatgatgattcccag-3′; reverse, 5′-ggacctcagttccgatga-3′), *m116HG* (forward, 5′-ggttgcattccctttccagtatg-3′; reverse, 5′-cagcaattcccatgttccttacc-3′), *mUbe3a*-ATS (forward, 5′-acagaacaataggtcaccaggtt-3′; reverse, 5′-aagcaagactgttcacctcat-3′), *GFP* (forward, 5′-acatgaagcagcacgacttct-3′; reverse, 5′-gacgttgtggctgttgtagttgta-3′) and *GAPDH* (forward, 5′-ggcaaattcaacggcacagt-3′; reverse, 5′-gggtctcgctcctggaagat-3′).

Bisulfite genomic sequencing

We isolated genomic DNA from human PWS fibroblasts or mouse tissues at P14 or P15. We treated DNA (1 μg) with bisulfite using the Epi-Tect bisulfite kit (Qiagen), and we used 125 ng of input DNA per PCR amplification. We subcloned PCR products into pGEM-T easy vector (Promega), and we sequenced an average of 15 clones. We analyzed DNA-sequencing results using BISMA web-based analysis platform (http://services.ibc.uni-stuttgart.de/BDPC/BISMA/) with a setting for individual clones with <95% bisulfite conversion and <90% sequence identity to be excluded in the analysis. The primers that we used in this study are listed here. *SNRPNbis* (forward, 5′-ggtggttttttttaagagatagtttggg-3′; reverse, 5′-catccccctaatccactaccataac-3′), *Snrpnbis-outer* (forward, 5′-tatgtaatatgatatagtttagaaattag-3′; reverse, 5′-aataaacccaaatctaaaatattttaatc-3′) and *Snrpnbis-inner* (forward, 5′-aatttgtgtgatgtttgtaattatttgg-3′; reverse, 5′-ataaaatacactttcactactaaaatcc-3′).

Chromatin immunoprecipitation assay

We analyzed histone methylations on the SNRPN locus in human fibroblasts by chromatin immunoprecipitation assay (ChIP) using the protocol as previously reported[14,15,37]. We performed ChIP assay using the ChIP-IT Express magnetic kit (Active Motif) according to the manufacturer's instructions, with modification for the fixation and reverse-cross-linking steps. Briefly, we prepared native chromatin without fixation and enzymatic digestions to average 150–500-bp-sized chromatin. We added 20 μg of chromatin to the specific antibodies (2 μg) or species control isotype antibodies for each immunoprecipitation reaction. We incubated the antibody-chromatin complexes with protein G magnetic beads for recovering chromatin immunoprecipitates. We purified RNase- and proteinase K–treated DNA using PCR purification columns (Promega). We quantified DNA recovery through real-time PCR performed on the LightCycler480 instrument (Roche) using SsoAdvanced Universal SYBR green Supermix (Biorad). We used the following antibodies: anti-rabbit acetylated H3 (Millipore 06-599), anti-mouse monoclonal histone H3 dimethyl K9 (Abcam 1220) and histone H3 trimethyl K9 (Millipore, 07-442), EHMT2/G9a (Abcam ab40542). We performed qPCR reactions with the following cycling parameters: at 95 °C/5 min followed by 40 cycles of 95 °C/30 s, 60 °C/60 s. We normalized data to the total input. The primers that we used in this study are listed here. *MAGEA2* (forward, 5′-gcctcaggatccccgtcccaat-3′; reverse, 5′-tggaaccggattctgcccggat-3′), *CEN* (forward, 5′-gtctctttcttgtttttaagctggg-3′; reverse, 5′-tgagctcattgagacatttgg-3′), *NDN* (forward, 5′-taaccctgttttccaggtatgg-3′; reverse, 5′-aagctgctgatgagaagaaacc-3′), *PWS-IC* (forward, 5′-ctagaggccccctctcattgcaac-3′; reverse, 5′-cttcgcacacatccccgcctgagc-3′), *SNORD116* (forward, 5′-tcttcaaatgtgcttggatcga-3′; reverse, 5′-tcttcaaatgtgcttggatcga-3′), *U-SNRPN* (forward, 5′-caatggaccaagagcattgata-3′; reverse, 5′- atagggtattgaaaccccgagt-3′), *SNORD116dw* (forward, 5′-tgagtcccacaaggaagtttttt-3′; reverse, 5′-acattcaaagaggcaggacatt-3′), *UBE3A* (forward, 5′-ttgcttcctgagcaagtcataa-3′; reverse, 5′-tccgaaagcatgacatatcaac-3′), rhodopsin (forward, 5′-

caagtcatgcagaagttagggg-3′; reverse, 5′-acccttataaagtgacctcccc-3′) and *GAPDH* (forward, 5′-gcatcacccggaggagaaaatcgg-3′; reverse, 5′-gtcacgtgtcgcagaggagc-3′).

Chromatin accessibility assay

We performed a chromatin-accessibility assay to investigate whether G9a inhibitors change the open or closed state of the imprinted cluster in the PWS-IC region, according to the previous report[44], with slight modifications. Briefly, 3 d after drug treatment in human PWS fibroblasts, we harvested the cells and lysed with lysis buffer (0.5% NP-40, 15 mM Tris-HCl (pH 7.4), 0.15 mM spermidine, 0.5 mM spermine, 15 mM NaCl, 60 mM KCl, 1 mM DTT, 0.1mM PMSF, 0.5-M sucrose, protease and phosphatase inhibitor cocktail (Roche)). We collected the lysed cells by centrifugation (3,000 r.p.m./10 min/4 °C) and rinsed with digestive buffer (15 mM Tris-HCl (pH 7.4), 15 mM NaCl, 60 mM KCl, 4 mM $MgCl_2$, 1 mM DTT, 0.1 mM PMSF, 0.35 M sucrose). After rinsing the cell pellets, we added MNase (NEB) to digest the open status of chromatins, followed by genomic qPCR to determine changes in amount of *SNRPN* and other imprinted genes. We defined chromatin accessibility using ΔCt, CtNuc(+) – CtNuc(−). The primers that we used in this study are described under ‘Chromatin immunoprecipitation assay.’

Statistical analysis

We used Graphpad Prism (Graphpad Software) for the statistical analyses. We used Student’s *t* test to examine the statistical significance between groups (vehicle controls versus drug-treated experiments). Data from multiple independent experiments were assumed to be of normal variance. No statistical method was used to predetermine sample size. Student’s *t* test (paired or unpaired, as appropriate) was used in Figures 1e, 2e, 3d, 4c,d,g, 5a,c–e and 6b and Supplementary Fig. 6b, 8 and 9a,b. $P < 0.05$ was considered to be statistically significant. For the comparison of survival rates after drug treatment, we used the Kaplan–Meier log–rank test. For the comparison of body weight, first we used Student’s *t* test (unpaired) to examine the statistical significance between groups (vehicle controls versus drug-treated experiments) in Figure 3d. Then we used two-way ANOVA to test significance in drug treatment and genotype, including *F* test to determine samples with unequal variance. *P* and *F* values are indicated in the legend of Figure 3e. Body-weight data, from P7 to P10 and from P20 to P25 mice, were excluded owing to the period of drug administration and small samples size of PBS_PWS ($n = 2$), respectively. For the comparison of chromatin accessibility, first we used two-way ANOVA to examine the statistical significance in drug treatment and nuclease digestion, including an *F* test to determine samples with unequal variance. *P* and *F* values are indicated in the legend of Supplementary Figure 10. Then, we used Student’s *t* test to examine between groups (vehicle controls versus drug-treated experiments) in Figure 6b. ANOVA Dunnett was used in Supplementary Figure 3b. Data from multiple independent experiments was assumed to be normal variance. All data were expressed as means ± s.e.m., mean % of fluorescence intensity (FI) or means with max and min, as indicated. The number of mice (or cell cultures) in each experimental group is indicated in the figure description. Sample sizes were determined on the basis of review of similar experiments in in literature[22,23,31,34]. No data points were excluded, except two-way ANOVA in the comparison of body weight, as described above.

Supplementary Material

Refer to Web version on PubMed Central for supplementary material.

Acknowledgments

We thank A. Beaudet at Baylor College of Medicine for providing the Snrpn-EGFP mice and some of the PWS cell lines; B. Philpot and M. Zlyka (University of North Carolina at Chapel Hill) for discussion. K. Konze for his advice on the ChIP experiment; S.-O. Han for his advice on blood-sample collection; C. Means and R. Rodriguiz for their assistance with neurological screening; and A. Bey for proofreading and discussion. This study is supported by grants from the US National Institutes of Health (HD077197 to Y.-H.J. and R01GM103893 to J.J.). Y.-H. Jiang is also supported by a grant from the Foundation for Prader–Willi Syndrome Research (FPWR). We thank the International Rett Syndrome Foundation and GlaxoSmithKline for providing the CNS-penetrating drug library (SMART library) and Published Kinase Inhibitor Set (PKIS), the NIMH Psychoactive Drug Screening Program (B.L. Roth) and the Michael Hooker Chair of Translational Proteomics (B.L. Roth).

References

1. Cassidy SB, Driscoll DJ. Prader–Willi syndrome. Eur J Hum Genet. 2009; 17:3–13. [PubMed: 18781185]
2. Buiting K. Prader-Willi syndrome and Angelman syndrome. Am J Med Genet C Semin Med Genet. 2010; 154C:365–376. [PubMed: 20803659]
3. Sahoo T, et al. Prader-Willi phenotype caused by paternal deficiency for the HBII-85 C/D box small nucleolar RNA cluster. Nat Genet. 2008; 40:719–721. [PubMed: 18500341]
4. de Smith AJ, et al. A deletion of the HBII-85 class of small nucleolar RNAs (snoRNAs) is associated with hyperphagia, obesity and hypogonadism. Hum Mol Genet. 2009; 18:3257–3265. [PubMed: 19498035]
5. Duker AL, et al. Paternally inherited microdeletion at 15q11.2 confirms a significant role for the SNORD116 C/D box snoRNA cluster in Prader-Willi syndrome. Eur J Hum Genet. 2010; 18:1196–1201. [PubMed: 20588305]
6. Bieth E, et al. Highly restricted deletion of the SNORD116 region is implicated in Prader-Willi Syndrome. Eur J Hum Genet. 2015; 23:252–255. [PubMed: 24916642]
7. Buiting K, et al. Clinical phenotypes of MAGEL2 mutations and deletions. Orphanet J Rare Dis. 2014; 9:40. [PubMed: 24661356]
8. Schaaf CP, et al. Truncating mutations of MAGEL2 cause Prader-Willi phenotypes and autism. Nat Genet. 2013; 45:1405–1408. [PubMed: 24076603]
9. Kanber D, et al. A paternal deletion of MKRN3, MAGEL2 and NDN does not result in Prader-Willi syndrome. Eur J Hum Genet. 2009; 17:582–590. [PubMed: 19066619]
10. Runte M, et al. The IC-SNURF-SNRPN transcript serves as a host for multiple small nucleolar RNA species and as an antisense RNA for UBE3A. Hum Mol Genet. 2001; 10:2687–2700. [PubMed: 11726556]
11. de los Santos T, Schweizer J, Rees CA, Francke U. Small evolutionarily conserved RNA, resembling C/D box small nucleolar RNA, is transcribed from PWCR1, a novel imprinted gene in the Prader-Willi deletion region, which Is highly expressed in brain. Am J Hum Genet. 2000; 67:1067–1082. [PubMed: 11007541]
12. Gallagher RC, Pils B, Albalwi M, Francke U. Evidence for the role of PWCR1/ HBII-85 C/D box small nucleolar RNAs in Prader-Willi syndrome. Am J Hum Genet. 2002; 71:669–678. [PubMed: 12154412]
13. Saitoh S, et al. Minimal definition of the imprinting center and fixation of chromosome 15q11-q13 epigenotype by imprinting mutations. Proc Natl Acad Sci USA. 1996; 93:7811–7815. [PubMed: 8755558]
14. Fulmer-Smentek SB, Francke U. Association of acetylated histones with paternally expressed genes in the Prader–Willi deletion region. Hum Mol Genet. 2001; 10:645–652. [PubMed: 11230184]

15. Xin Z, Allis CD, Wagstaff J. Parent-specific complementary patterns of histone H3 lysine 9 and H3 lysine 4 methylation at the Prader-Willi syndrome imprinting center. Am J Hum Genet. 2001; 69:1389–1394. [PubMed: 11592036]
16. Saitoh S, Wada T. Parent-of-origin specific histone acetylation and reactivation of a key imprinted gene locus in Prader-Willi syndrome. Am J Hum Genet. 2000; 66:1958–1962. [PubMed: 10775525]
17. Xin Z, et al. Role of histone methyltransferase G9a in CpG methylation of the Prader-Willi syndrome imprinting center. J Biol Chem. 2003; 278:14996–15000. [PubMed: 12586828]
18. Auclair G, et al. EHMT2 directs DNA methylation for efficient gene silencing in mouse embryos. Genome Res. 2016; 26:192–202. [PubMed: 26576615]
19. Sutcliffe JS, et al. Deletions of a differentially methylated CpG island at the SNRPN gene define a putative imprinting control region. Nat Genet. 1994; 8:52–58. [PubMed: 7987392]
20. Le Meur E, et al. Dynamic developmental regulation of the large non-coding RNA associated with the mouse 7C imprinted chromosomal region. Dev Biol. 2005; 286:587–600. [PubMed: 16126194]
21. Wu MY, Tsai TF, Beaudet AL. Deficiency of Rbbp1/Arid4a and Rbbp1l1/Arid4b alters epigenetic modifications and suppresses an imprinting defect in the PWS/AS domain. Genes Dev. 2006; 20:2859–2870. [PubMed: 17043311]
22. Huang HS, et al. Topoisomerase inhibitors unsilence the dormant allele of Ube3a in neurons. Nature. 2011; 481:185–189. [PubMed: 22190039]
23. Vedadi M, et al. A chemical probe selectively inhibits G9a and GLP methyltransferase activity in cells. Nat Chem Biol. 2011; 7:566–574. [PubMed: 21743462]
24. Liu F, et al. Discovery of an in vivo chemical probe of the lysine methyltransferases G9a and GLP. J Med Chem. 2013; 56:8931–8942. [PubMed: 24102134]
25. Liu F, et al. Optimization of cellular activity of G9a inhibitors 7-aminoalkoxy-quinazolines. J Med Chem. 2011; 54:6139–6150. [PubMed: 21780790]
26. Kubicek S, et al. Reversal of H3K9me2 by a small-molecule inhibitor for the G9a histone methyltransferase. Mol Cell. 2007; 25:473–481. [PubMed: 17289593]
27. Leung DC, et al. Lysine methyltransferase G9a is required for de novo DNA methylation and the establishment, but not the maintenance, of proviral silencing. Proc Natl Acad Sci USA. 2011; 108:5718–5723. [PubMed: 21427230]
28. Martins-Taylor K, et al. Imprinted expression of UBE3A in non-neuronal cells from a Prader-Willi syndrome patient with an atypical deletion. Hum Mol Genet. 2014; 23:2364–2373. [PubMed: 24363065]
29. Boccaccio I, et al. The human MAGEL2 gene and its mouse homologue are paternally expressed and mapped to the Prader-Willi region. Hum Mol Genet. 1999; 8:2497–2505. [PubMed: 10556298]
30. Chamberlain SJ, et al. Induced pluripotent stem cell models of the genomic imprinting disorders Angelman and Prader-Willi syndromes. Proc Natl Acad Sci USA. 2010; 107:17668–17673. [PubMed: 20876107]
31. Tsai TF, Jiang YH, Bressler J, Armstrong D, Beaudet AL. Paternal deletion from Snrpn to Ube3a in the mouse causes hypotonia, growth retardation and partial lethality and provides evidence for a gene contributing to Prader-Willi syndrome. Hum Mol Genet. 1999; 8:1357–1364. [PubMed: 10400982]
32. Chamberlain SJ, Brannan CI. The Prader-Willi syndrome imprinting center activates the paternally expressed murine Ube3a antisense transcript but represses paternal Ube3a. Genomics. 2001; 73:316–322. [PubMed: 11350123]
33. Meng L, Person RE, Beaudet AL. Ube3a-ATS is an atypical RNA polymerase II transcript that represses the paternal expression of Ube3a. Hum Mol Genet. 2012; 21:3001–3012. [PubMed: 22493002]
34. Jiang YH, et al. Mutation of the Angelman ubiquitin ligase in mice causes increased cytoplasmic p53 and deficits of contextual learning and long-term potentiation. Neuron. 1998; 21:799–811. [PubMed: 9808466]
35. Epsztejn-Litman S, et al. De novo DNA methylation promoted by G9a prevents reprogramming of embryonically silenced genes. Nat Struct Mol Biol. 2008; 15:1176–1183. [PubMed: 18953337]

36. Tachibana M, Matsumura Y, Fukuda M, Kimura H, Shinkai Y. G9a/GLP complexes independently mediate H3K9 and DNA methylation to silence transcription. EMBO J. 2008; 27:2681–2690. [PubMed: 18818694]
37. Cruvinel E, et al. Reactivation of maternal SNORD116 cluster via SETDB1 knockdown in Prader-Willi syndrome iPSCs. Hum Mol Genet. 2014; 23:4674–4685. [PubMed: 24760766]
38. Tachibana M, et al. G9a histone methyltransferase plays a dominant role in euchromatic histone H3 lysine 9 methylation and is essential for early embryogenesis. Genes Dev. 2002; 16:1779–1791. [PubMed: 12130538]
39. Yokochi T, et al. G9a selectively represses a class of late-replicating genes at the nuclear periphery. Proc Natl Acad Sci USA. 2009; 106:19363–19368. [PubMed: 19889976]
40. Shinkai Y, Tachibana M. H3K9 methyltransferase G9a and the related molecule GLP. Genes Dev. 2011; 25:781–788. [PubMed: 21498567]
41. Collins RE, et al. The ankyrin repeats of G9a and GLP histone methyltransferases are mono- and dimethyllysine binding modules. Nat Struct Mol Biol. 2008; 15:245–250. [PubMed: 18264113]
42. Collins R, Cheng X. A case study in cross-talk: the histone lysine methyltransferases G9a and GLP. Nucleic Acids Res. 2010; 38:3503–3511. [PubMed: 20159995]
43. Bittencourt D, Lee BH, Gao L, Gerke DS, Stallcup MR. Role of distinct surfaces of the G9a ankyrin repeat domain in histone and DNA methylation during embryonic stem cell self-renewal and differentiation. Epigenetics Chromatin. 2014; 7:27. [PubMed: 25478012]
44. Pai CC, et al. A histone H3K36 chromatin switch coordinates DNA double-strand break repair pathway choice. Nat Commun. 2014; 5:4091. [PubMed: 24909977]
45. Yamasaki K, et al. Neurons but not glial cells show reciprocal imprinting of sense and antisense transcripts of Ube3a. Hum Mol Genet. 2003; 12:837–847. [PubMed: 12668607]
46. Galiveti CR, Raabe CA, Konthur Z, Rozhdestvensky TS. Differential regulation of non-protein coding RNAs from Prader-Willi Syndrome locus. Sci Rep. 2014; 4:6445. [PubMed: 25246219]
47. Wen B, Wu H, Shinkai Y, Irizarry RA, Feinberg AP. Large histone H3 lysine 9 dimethylated chromatin blocks distinguish differentiated from embryonic stem cells. Nat Genet. 2009; 41:246–250. [PubMed: 19151716]
48. Lu X, et al. Chemical modification-assisted bisulfite sequencing (CAB-Seq) for 5-carboxylcytosine detection in DNA. J Am Chem Soc. 2013; 135:9315–9317. [PubMed: 23758547]
49. Booth MJ, et al. Oxidative bisulfite sequencing of 5-methylcytosine and 5-hydroxymethylcytosine. Nat Protoc. 2013; 8:1841–1851. [PubMed: 24008380]
50. Huang Y, et al. The behaviour of 5-hydroxymethylcytosine in bisulfite sequencing. PLoS One. 2010; 5:e8888. [PubMed: 20126651]
51. Garcia-Manero G, et al. Randomized open-label phase II study of decitabine in patients with low- or intermediate-risk myelodysplastic syndromes. J Clin Oncol. 2013; 31:2548–2553. [PubMed: 23733767]
52. Treppendahl MB, Kristensen LS, Grønbæk K. Predicting response to epigenetic therapy. J Clin Invest. 2014; 124:47–55. [PubMed: 24382389]
53. Mackay DJ, et al. A maternal hypomethylation syndrome presenting as transient neonatal diabetes mellitus. Hum Genet. 2006; 120:262–269. [PubMed: 16816970]
54. Mackay DJ, et al. Hypomethylation of multiple imprinted loci in individuals with transient neonatal diabetes is associated with mutations in ZFP57. Nat Genet. 2008; 40:949–951. [PubMed: 18622393]
55. Carpenter AE, et al. CellProfiler: image analysis software for identifying and quantifying cell phenotypes. Genome Biol. 2006; 7:R100. [PubMed: 17076895]
56. Wang X, Xu Q, Bey AL, Lee Y, Jiang YH. Transcriptional and functional complexity of Shank3 provides a molecular framework to understand the phenotypic heterogeneity of SHANK3 causing autism and Shank3 mutant mice. Mol Autism. 2014; 5:30. [PubMed: 25071925]
57. Hatcher JP, et al. Development of SHIRPA to characterise the phenotype of gene-targeted mice. Behav Brain Res. 2001; 125:43–47. [PubMed: 11682092]

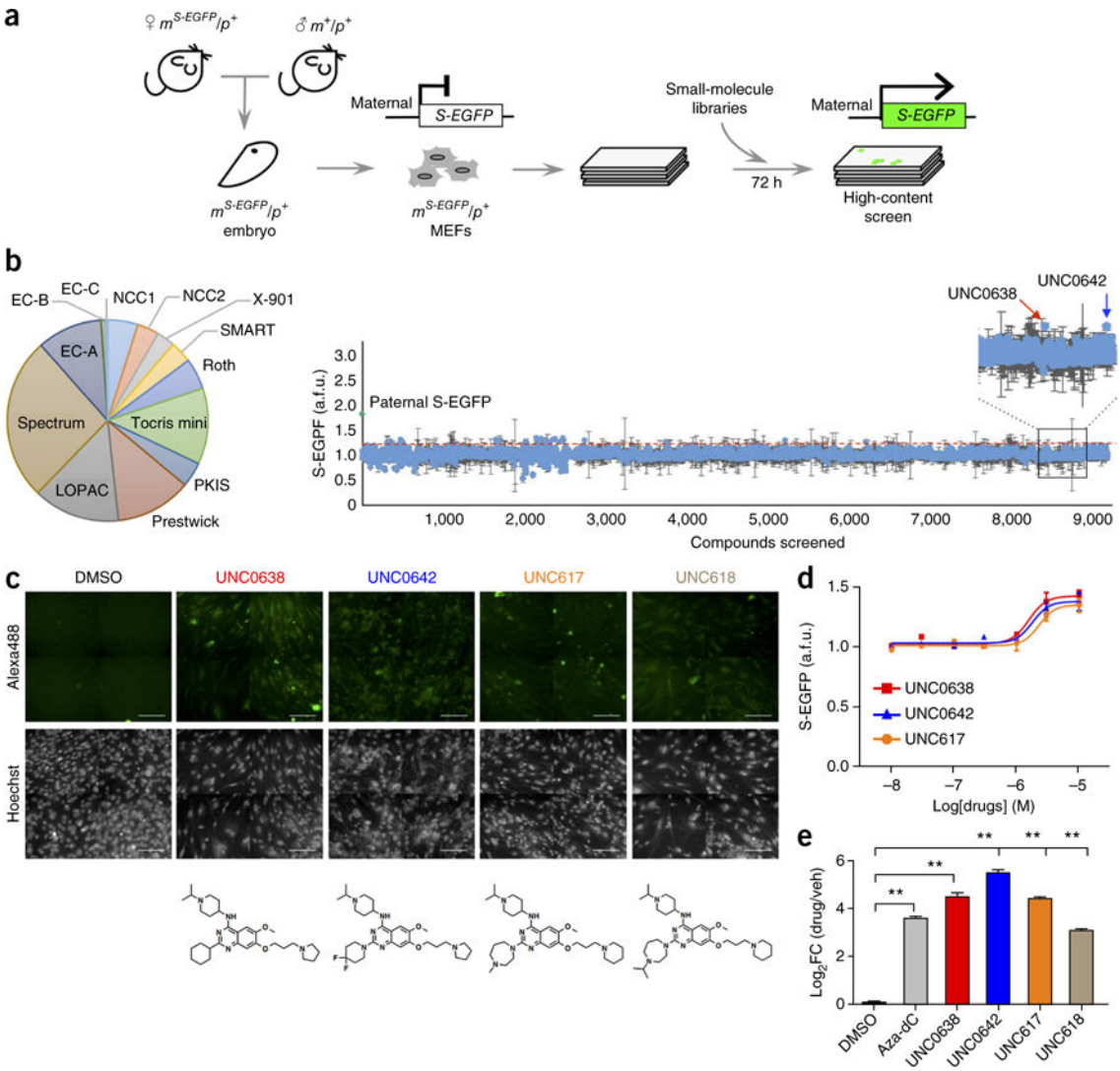

Figure 1.

Identification of small molecules that activate the expression of *Snrpn* from the maternal chromosome. (**a**) Screening strategy using a cell-based model. (**b**) Summary of all 9,157 compounds (pie chart, left) and data plot including constitutively active paternal S-EGFP as a positive control (dot plot, right). We highlighted two active compounds (data are mean % of fluorescence intensity (FI) ± s.e.m.; red dotted line indicates a cutoff of 1.25). (**c**) Representative images ($n = 4$ cultures for each drug tested) of maternal *Snrpn-EGFP* MEFs at the presence of the compounds and their chemical structures. Scale bars, 100 μm. (**d**) Concentration-response curves of UNC0638 (red), UNC0642 (blue) or UNC617 (orange) in maternal S-EGFP MEFs ($n = 4$ cultures per each point of dose; data are means ± s.e.m. of three independent experiments). (e) Validation of *Snrpn-EGFP* mRNA expressions in G9a inhibitor- or 5-Aza-dC-treated MEFs using RT–qPCR (Livak methods, normalization to β-actin, Student's *t* test; $^{**}P < 0.01$; $n = 4$ cultures per group, data are means ± s.e.m. of three independent experiments).

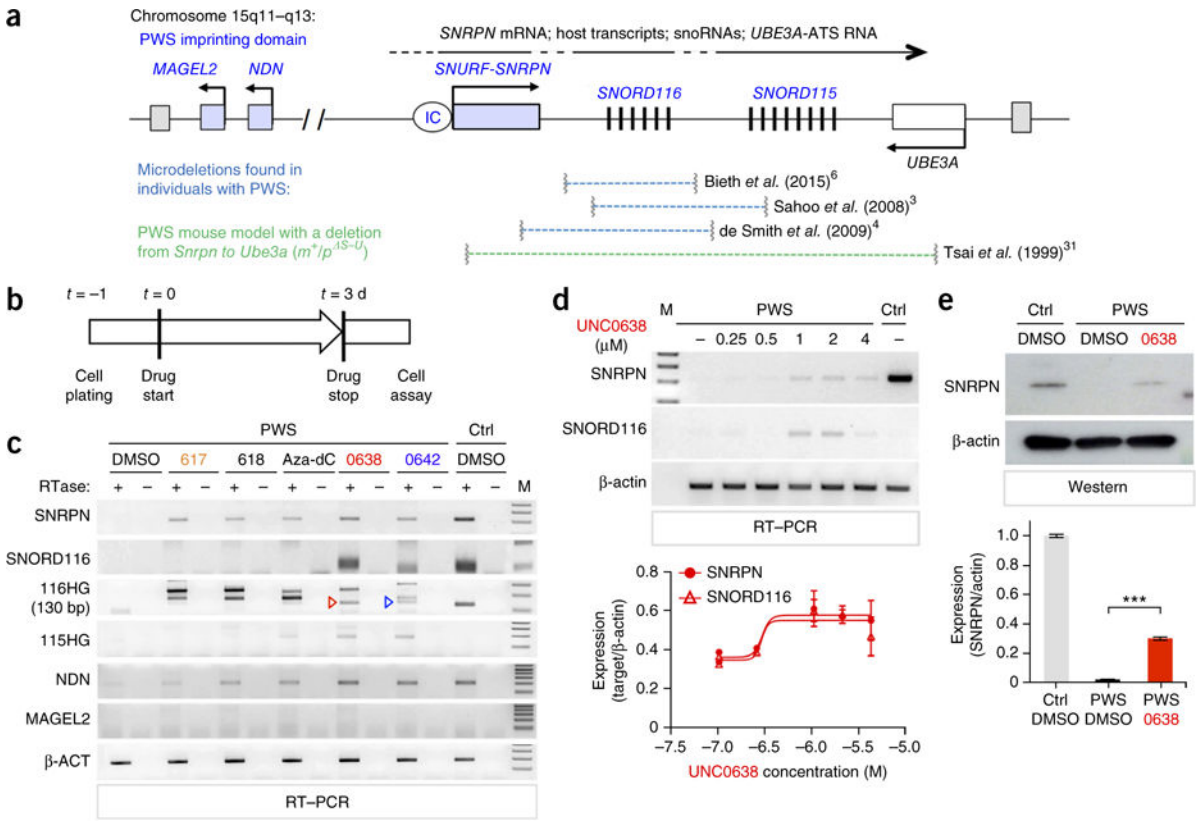

Figure 2.

UNC0638 activates the expression of candidate PWS-associated genes in fibroblasts derived from individuals with PWS. (**a**) Schematic of genomic organization of PWS-associated imprinted domain at the human chromosome 15q11–q13 (IC, imprinting center). (**b**) Schematic of *in vitro* treatment used in c–e. (**c**) Representative RT–PCR analysis ($n > 10$ independent experiments for *SNRPN* and *SNORD116* and $n = 3$ independent experiments for the other genes and transcripts from 15q11–q13) in human PWS fibroblasts treated with UNC0638, UNC0642, UNC617, UNC618 or 5-Aza-dC (ctrl, control; *116HG*, host transcript for *SNORD116*; *115HG*, host transcript of *SNORD115*; RTase: +/−, with or without reverse transcriptase; M, 1kb DNA ladder). (**d**) Representative RT–PCR ($n > 10$ for *SNRPN* and *SNORD116*) (top) and concentration-response curves (bottom; $n = 3$ cultures per each point of dose; data are means ± s.e.m. of two independent experiments) of *SNRPN* and *SNORD116* in UNC0638-treated human fibroblasts. UNC0638 activated the expression of *SNRPN* and *SNORD116* in PWS fibroblasts (PWS cell line derived from an individual with PWS carrying a 6-Mb paternal deletion of chromosome 15q11–q13; ctrl, from an individual without PWS; M, 1-kb DNA ladder). (**e**) Cropped representative western blot ($n = 3$ cultures per group of two independent experiments) (top; the original blot is shown in Supplementary Fig. 4) and quantification of the *SNRPN* protein (bottom) in human PWS fibroblasts with or without UNC0638 (0638) treatment. Student's *t*-test; $***P < 0.0001$; data are means ± s.e.m.

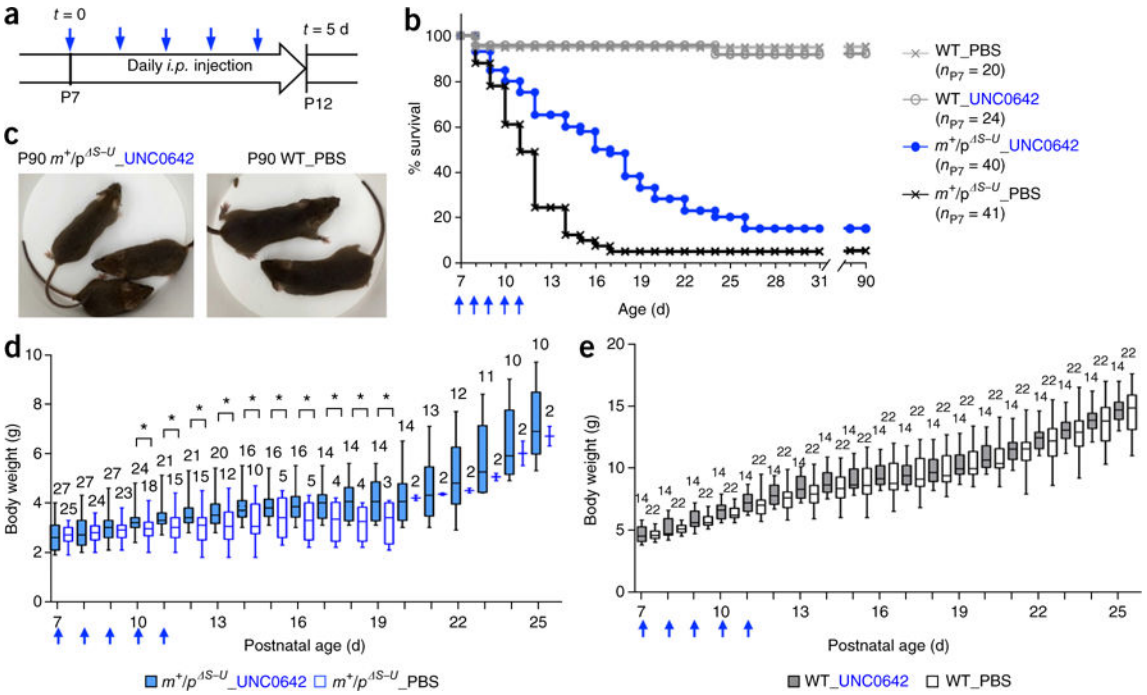

Figure 3.

UNC0642 improves survival and growth in a mouse model with a paternal deletion from *Snrpn* to *Ube3a* ($m^+/p^{\Delta S-U}$). (**a**) Schematic of *in vivo* treatment of $m^+/p^{\Delta S-U}$ mice in **b–e**. (**b**) Improved survival of UNC0642-treated $m^+/p^{\Delta S-U}$ pups (Kaplan–Meier log–rank test, $P = 0.001$; $\chi 2 = 15.0039$; df = 1; data are percentage of survival). (**c**) The normal appearance of UNC0642-treated $m^+/p^{\Delta S-U}$ and PBS-treated wild-type (WT) mice at P90. (**d**) Changes in weight gain in $m^+/p^{\Delta S-U}$ mice with or without the treatment of UNC0642. Box-and-whisker plots correspond to body weight of PBS-treated $m^+/p^{\Delta S-U}$ (open blue, $n = 25$ mice at P7 and $n = 2$ mice at P25); UNC0642-treated $m^+/p^{\Delta S-U}$ (blue, $n = 27$ mice at P7 and $n = 6$ mice at P25) (Student's t test; $^*P < 0.05$; between two groups of PWS_UNC0642 and PWS_PBS from P10 to P19). (e) Changes in weight gain in WT mice with or without the treatment of UNC0642 (open black line, $n = 22$ mice at P7 and $n = 22$ mice at P25); treated WT (black, $n = 14$ mice at P7 and $n = 14$ mice at P25). Two-way ANOVA; treatment; $P < 0.0001$; $F = 863.3$, genotype; $P < 0.0001$; $F = 14.86$, interaction; $P < 0.0001$; $F = 2.86$ from P10 to P19; data are means with max and min.

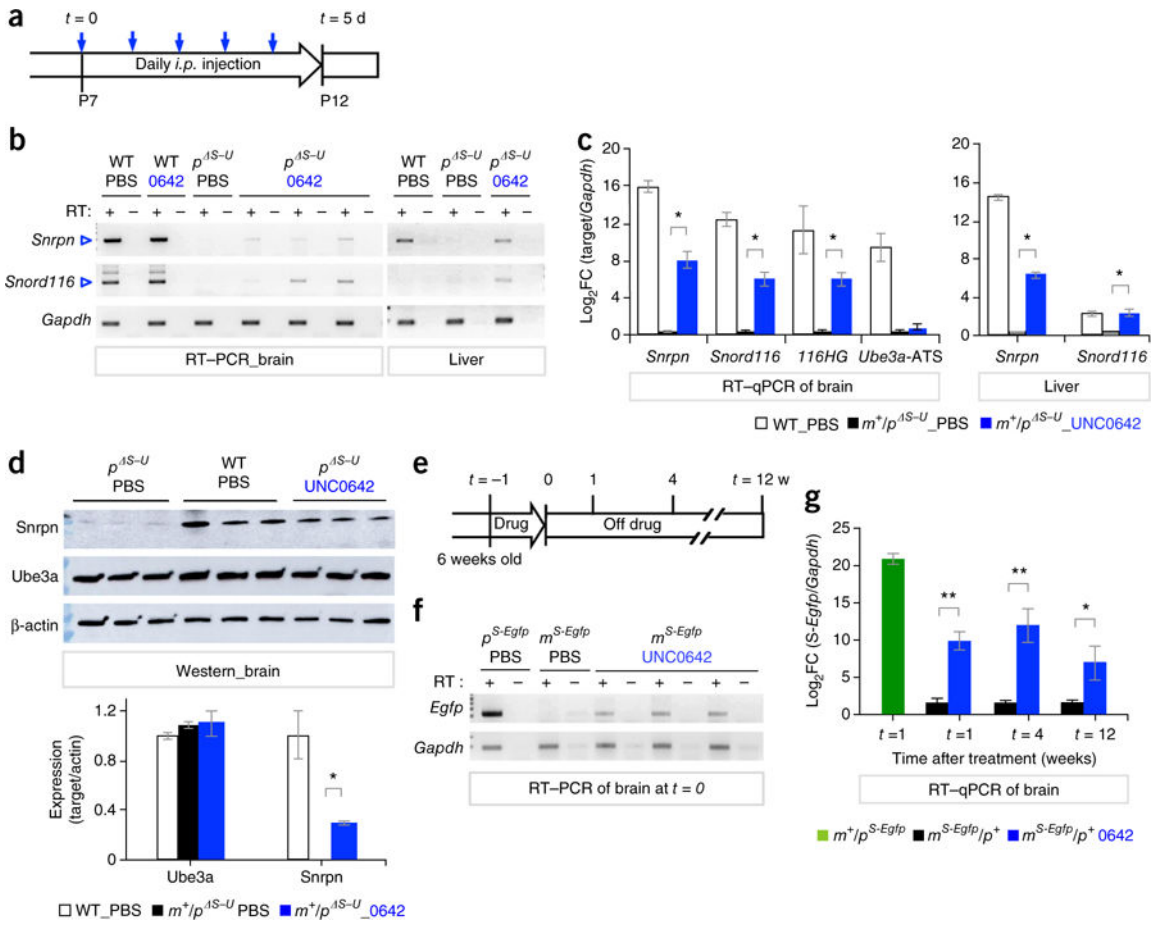

Figure 4.

UNC0642 activates candidate PWS-associated genes in mouse models with a paternal deletion from *Snrpn* to *Ube3a* ($m^{+}/p^{\Delta S-U}$). (a) Schematic of *in vivo* treatment of $m^{+}/p^{\Delta S-U}$ mice for **b**, **c**, and **d**. (**b**) Representative RT–PCR analysis of *Snrpn* and *Snord116* in the brain and the liver in a mouse model of PWS treated with UNC0642. UNC0642 activated the expression of *Snrpn* and *Snord116* (RT: +/−, with or without reverse transcriptase; three independent experiments). (**c**) Representative RT–qPCR analysis ($n = 4$ mice per group from six independent experiments for *Snrpn* and *Snord116* and three independent experiments for *116HG* and *Ube3a*-ATS) of the brain and the liver in mouse models of PWS treated with UNC0642. UNC0642 activated *Snrpn*, and *Snord116*, but not *Ube3a*-ATS (Student's *t* test; $^{*}P < 0.05$; $n = 4$ per group, data are mean ± s.e.m.). (**d**) Cropped representative western blot analysis ($n = 3$ mice per group with two independent experiments) (top; the original blot is shown in Supplementary Fig. 6a) and quantification (bottom; expression levels were normalized to β-actin). The level of SNPRN but not UBE3A protein was significantly increased after treatment (Student's *t* test; $^{*}P < 0.05$; $n = 3$ per group, data are means ± s.e.m. two independent experiments). (**e**) Schematic of treatment in 6-week-old mice for examining long-term activation of maternal genes in **f** and **g**. (**f**) Representative RT–PCR analysis ($n = 3$ mice per group, with three independent experiments) of *S-EGFP* in the brains of mice carrying imprinted *S-EGFP*. UNC0642 derepressed *S-EGFP* after 1 week of treatment (RT: +/−, with or without reverse transcriptase; three independent experiments).

(**g**) Representative RT–qPCR analysis (n = 3–5 mice per group, with two independent experiments) of *S-EGFP* in the brains of mice carrying imprinted *S-EGFP*. Student's t test; $*P < 0.05$; $**P < 0.01$; data are means ± s.e.m.

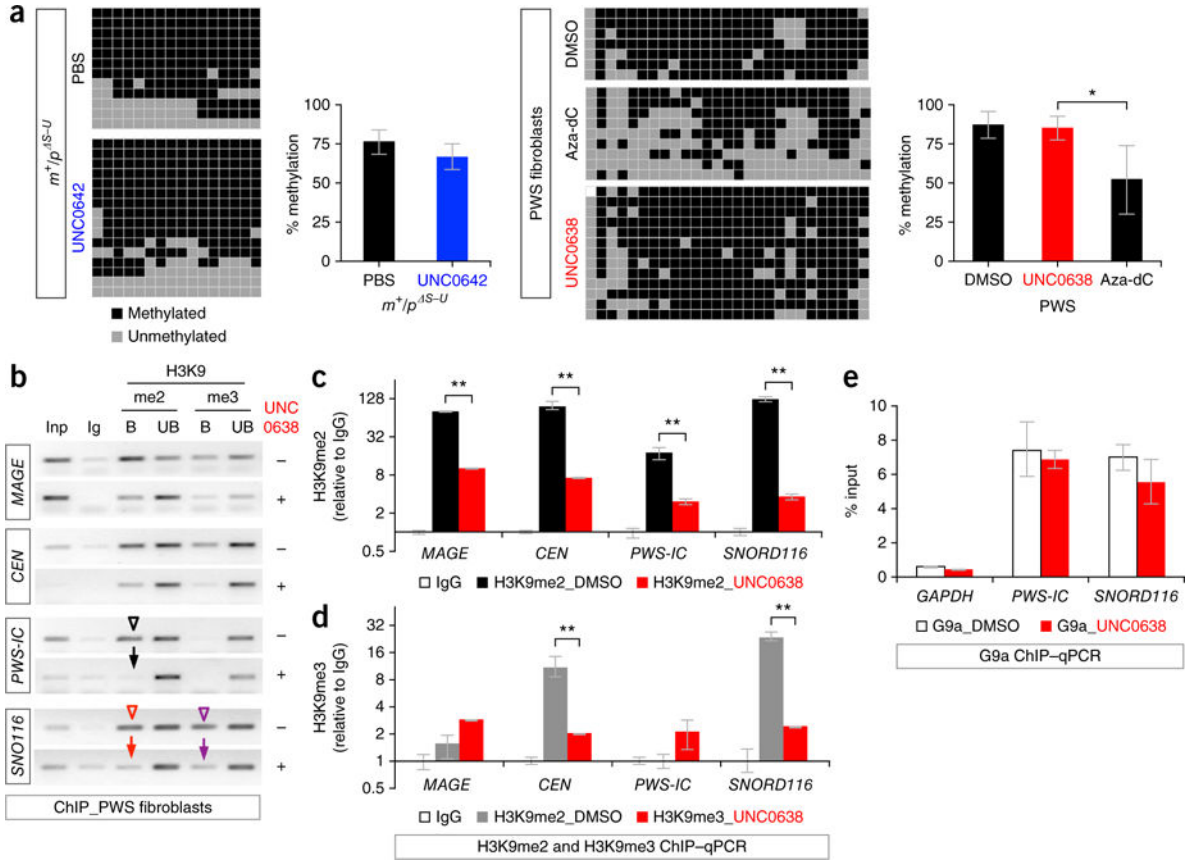

Figure 5.

The activation of candidate PWS-associated genes by UNC0638 and UNC0642 is associated with demethylation of H3K9. (**a**) Comparison of the DNA methylation in PWS-IC between vehicle- and UNC0642- or UNC0638- treated in liver of $m^{+}/p^{\Delta s-u}$ mice and in a human PWS fibroblast cell lines. Left, black square indicates methylated, and gray square unmethylated, CpG sites. Right, the average methylation measured by the number of methylated CG sites divided by the total number of CG sites analyzed (Student's *t* test; $*P < 0.05$; $n = 7–16$ clones per group; data are means ± s.e.m. of three independent experiments). (**b–d**) Changes in repressive histone marks associated with the activation of the maternal *SNRPN* and *SNORD116* in PWS fibroblasts. (**b**) Genomic DNA PCR following chromatin immunoprecipitation of H3K9me2 or H3K9me3 in PWS fibroblasts. The recovery of DNA indicates its binding with the histone modification in the absence (open arrowheads) or presence (arrows) of UNC0638 as both *MAGE-A2* (*MAGE*) and centromere (*CEN*) serve as control (Inp, input; Ig, IgG isotype control; K9me2, histone H3 lysine 9 dimethylation; K9me3, histone H3 lysine 9 trimethylation; B, bound fraction; UB, unbound fraction). (**c**,d) ChIP–qPCR quantification of H3K9me2 (**c**) and H3K9me3 (**d**). Data showed the enrichment over IgG and the fold change of H3K9me2 and H3K9me3 in UNC0638-treated cells. (**c**; K9me2/$\log_2$FC: Student's *t* test; $**P < 0.01$; $n = 3$ cultures per group, data are means ± s.e.m. of three independent experiments. **d**; K9me3/$\log_2$FC: Student's *t* test; $**P < 0.01$; $n =$ 3 cultures per group, data are means ± s.e.m. of three independent experiments). (**e**) Stable G9a binding in ChIP. G9a binding was not changed in the PWS fibroblasts treated with

UNC0638 (Student's *t* test); $n = 3$ cultures per group, data are means ± s.e.m. of two independent experiments).

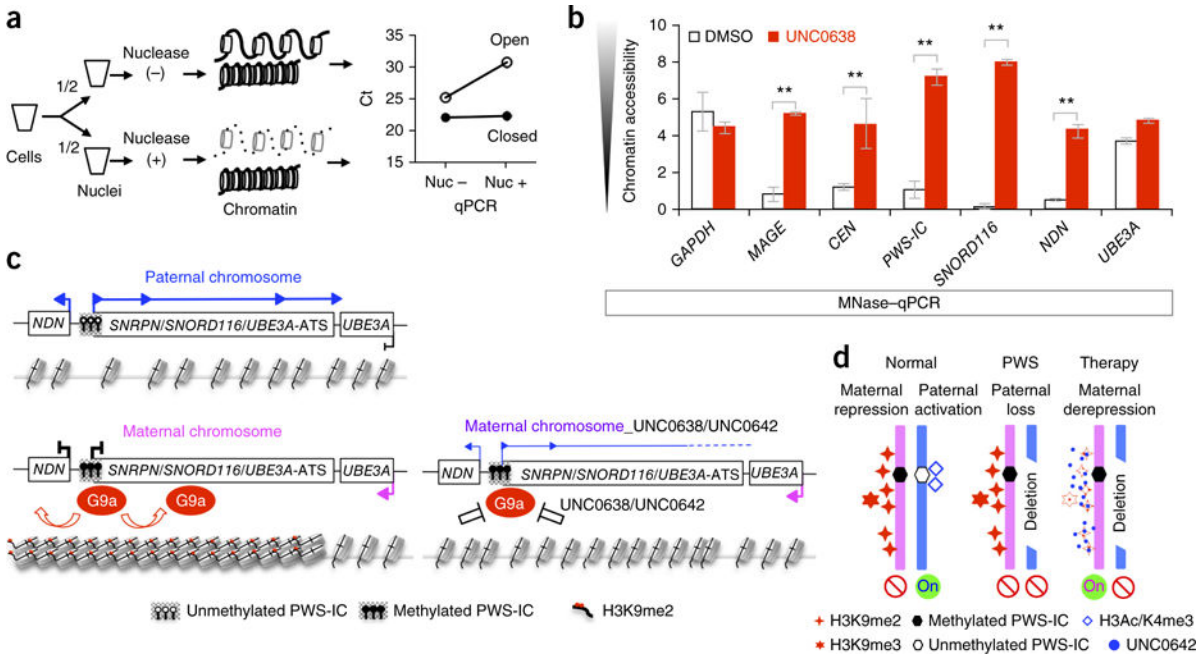

Figure 6.

Activation of candidate PWS-associated genes by UNC0638 and UNC0642 is associated with enhanced chromatin accessibility. (**a**) Experimental scheme for assessing chromatin accessibility. (**b**) Increased chromatin accessibility in the PWS imprinted domain by UNC0638. *GAPDH* (active) and rhodopsin (silent) genes serve as controls for chromatin that is highly susceptible versus resistant to nuclease digestion (data set of nuclease sensitivity shown in Supplementary Fig. 10). The chromatin at the genomic loci of PWS-IC, *SNORD116* and *NDN*, but not *UBE3A*, was more accessible after UNC0638 treatment. (GAP, *GAPDH*; Nuc, Nuclease; Chr, chromatin. Student's *t* test; $^{**}P < 0.01$; $n = 3$ cultures per group, data are means ± s.e.m. of two independent experiments). (**c**) A schematic chromatin-spreading model for maternal activation of the candidate PWS-associated genes in response to G9a inhibitor. Top, on the paternal chromosome, a widely open chromatin structure allows for gene transcription (for example, *NDN, SNRPN* and *SNORD116*). Bottom left, on the maternal chromosome, G9a-mediated methylation of H3K9 can propagate in a bidirectional manner along the PWS-associated genes. A compact, closed chromatin structure suppresses gene transcription of paternally expressed genes. Bottom right, UNC0642 or UNC0638 induces the opening of chromatin structure through the reduction of H3K9 methylation, which derepresses the expression of PWS-associated genes. (**d**) A proof of principle of epigenetic therapy for PWS via the G9a inhibitor. UNC0638 and UNC0642 (blue dots) directly reduce H3K9 methylation (red stars), but do not change methylated PWS-IC (black hexagon). The reduction of H3K9 methylation would be sufficient to activate PWS-associated genes, and thereby offer therapeutic benefits.